

## Accepted Manuscript

Title: Highly efficient transformation of  $\gamma$ -valerolactone to valerate esters over structure-controlled copper/zirconia catalysts prepared via a reduction-oxidation route

Authors: Shanshan Liu, Guoli Fan, Lan Yang, Feng Li



PII: S0926-860X(17)30281-8  
DOI: <http://dx.doi.org/doi:10.1016/j.apcata.2017.06.032>  
Reference: APCATA 16294

To appear in: *Applied Catalysis A: General*

Received date: 16-3-2017  
Revised date: 16-6-2017  
Accepted date: 22-6-2017

Please cite this article as: Shanshan Liu, Guoli Fan, Lan Yang, Feng Li, Highly efficient transformation of  $\gamma$ -valerolactone to valerate esters over structure-controlled copper/zirconia catalysts prepared via a reduction-oxidation route, *Applied Catalysis A, General* <http://dx.doi.org/10.1016/j.apcata.2017.06.032>

This is a PDF file of an unedited manuscript that has been accepted for publication. As a service to our customers we are providing this early version of the manuscript. The manuscript will undergo copyediting, typesetting, and review of the resulting proof before it is published in its final form. Please note that during the production process errors may be discovered which could affect the content, and all legal disclaimers that apply to the journal pertain.

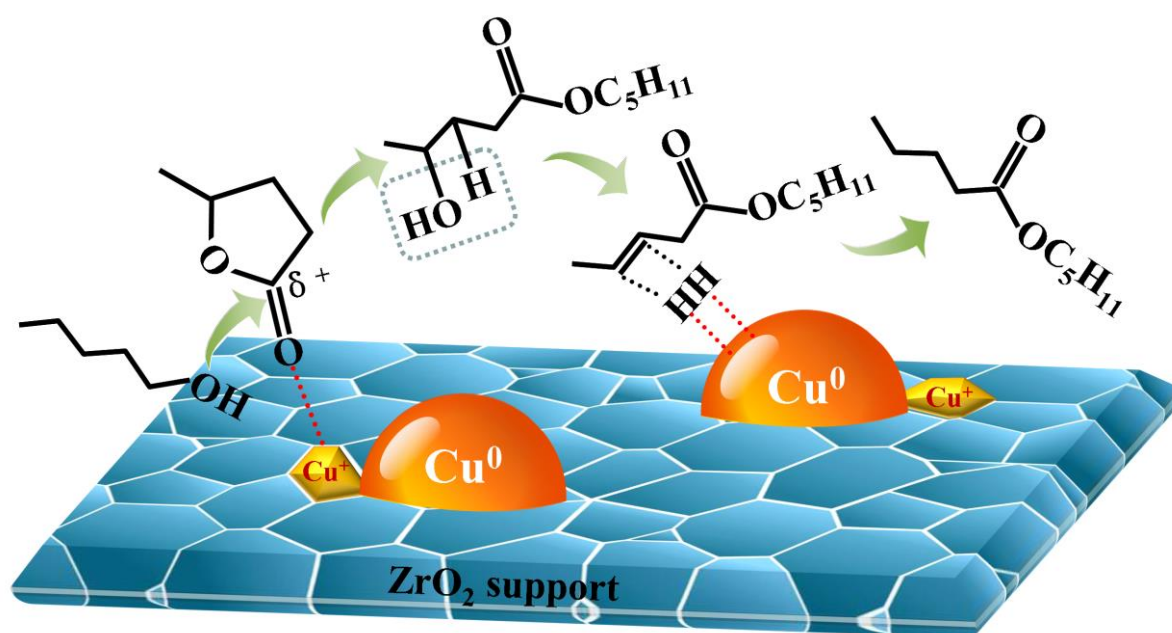
# Highly efficient transformation of $\gamma$ -valerolactone to valerate esters over structure-controlled copper/zirconia catalysts prepared via a reduction-oxidation route

Shanshan Liu, Guoli Fan,\* Lan Yang, Feng Li \*

State Key Laboratory of Chemical Resource Engineering, Beijing Advanced Innovation Center for Soft Matter Science and Engineering, Beijing University of Chemical Technology, P.O. Box 98, No.15 Beisanhuan Donglu, Beijing 100029, P.R. China. Tel.: 8610-64451226; Fax: 8610-64425385.

Email: [fangl@mail.buct.edu.cn](mailto:fangl@mail.buct.edu.cn) (G.Fan); [lifeng@mail.buct.edu.cn](mailto:lifeng@mail.buct.edu.cn) (F.Li)

Graphical abstract



## Highlights

- Novel reduction-oxidation route for the synthesis of Cu/ZrO<sub>2</sub> catalysts is established
- Metal-support interaction is responsible for the formation of surface Cu<sup>+</sup>
- Porous structure of ZrO<sub>2</sub> support inhibits the aggregation of Cu species
- Cooperation of Cu<sup>0</sup> and Cu<sup>+</sup> is crucial for achieving high catalytic performance

## Abstract

Design and development of novel and efficient catalysts are crucial but challenging for the catalytic conversion of biomass and derivatives to fuels and chemicals. In this paper, a novel separate nucleation and aging steps assistant reduction-oxidation strategy was developed to synthesis CuO/ZrO<sub>2</sub> complex precursor with homogeneously distributed Cu and Zr components, which can be used as an ideal precursor for the synthesis of highly dispersed Cu/ZrO<sub>2</sub> catalyst. Characterization results revealed that homogeneous dispersion of CuO, high surface area of ZrO<sub>2</sub> support with controlled porous structure, and strong interaction between CuO and ZrO<sub>2</sub> in CuO/ZrO<sub>2</sub> precursor could lead to the enhanced Cu dispersion and the formation of Cu<sup>+</sup> active centers. The synthesized Cu/ZrO<sub>2</sub> catalysts exhibited excellent

catalytic performance (85.4% conversion of GVL and 98.0% selectivity of pentyl valerate) in the catalytic transformation of GVL to valerate esters, more efficient than that of Cu/ZrO<sub>2</sub>-CP and Cu/ZrO<sub>2</sub>-CH catalysts prepared via co-precipitation and chemisorption hydrolysis methods, respectively. The superior catalytic performance was mainly attributed to both the cooperation of Cu<sup>0</sup> and Cu<sup>+</sup> species and the highly dispersed surface Cu<sup>0</sup>, thereby improving the adsorption and polarization of C=O bond in GVL and the following dissociation of H<sub>2</sub> to produce active hydrogen for the hydrogenation step during the catalytic transformation of GVL. Moreover, such copper-based catalysts exhibited potential applications in the exploitation and utilization of biomass resources with significantly enhanced efficiency.

**Keywords:** copper/zirconia catalyst; reduction-oxidation route; metal-support interaction; valerate esters; biomass-conversion.

## 1. Introduction

Urged by the decreasing fossil resources and growing environmental concerns, tremendous efforts have been devoted to exploiting economically efficient and environmental friendly technologies to use biomass as feedstock for the production of bio-based platform molecules and convert these molecules into desired value-added chemicals [1-4]. Among these molecules,  $\gamma$ -valerolactone (GVL), a colorless liquid with a sweet and herbaceous odor, obtained from C6 and C5 sugars through levulinic acid (LA) intermediate [5-12], has been identified as a promising fuel additive; meanwhile, it can also be used as one of the most promising platform intermediate to produce biofuels [13-15], solvents [16-18], polymers [19, 20], and fine chemicals [21-24].

Among the fine chemicals generated by the catalytic transformation of GVL, alkyl valerates have been extensively studied and used as oxygenic fuel components for gasoline and diesel fuels because of their unique properties such as low polarity, higher energy density, and less miscible with water [5, 25]. Lange et al did some pioneering works and reported that

GVL can be converted directly into pentyl valerate over Pt/TiO<sub>2</sub> or Pd/TiO<sub>2</sub> catalyst at 275-300 °C with unsatisfactory selectivity [26]. Sun et al reported an efficient bi-functional base-metal catalyst (Co/HZSM-5) for the conversion of GVL in ethanol solvent with ethyl valerate selectivity up to 64.2% [27]. Recently, Cu-based catalysts, a kind of candidates for the substitution of noble-metal catalysts, have exhibited extraordinary catalytic performance in the catalytic transformation of GVL. For example, Ravasio et al developed a chemisorptions-hydrolysis method for the preparation of Cu/SiO<sub>2</sub> catalysts and tested their catalytic activity for one-pot transformation of GVL into pentyl valerate at 250 °C using pentanol as solvent. They found that small Cu particles were acted as Lewis acid sites to activate GVL and were primarily responsible for the excellent catalytic performance with GVL conversion over 91% and pentyl valerate selectivity up to 92 % [28]. Chan-Thaw et al explored Cu/SiO<sub>2</sub>-ZrO<sub>2</sub> catalysts and investigated their catalytic performance for the production of pentyl valerate and ethyl valerate from GVL. They found that the use of ethanol as solvent resulted the extra formation of ethyl 4-ethoxy pentanoate and pentenoic esters byproducts, thus leading the low selectivity of ethyl valerate [29]. Up to now, the overall yield of valerate esters over Cu-based catalyst is still low and many processes are required to be integrated urgently.

In the past decades, Cu-based catalysts have been prepared by various methods including oxalate gel-coprecipitation method [30], co-precipitation [31, 32], impregnation [33] and chemisorption hydrolysis [34]. Despite the above-mentioned methods which were used to prepare Cu-based catalyst with improved catalytic performance, in most cases, their synthetic process often suffers from drawbacks such as low time efficiency, complicated fabrication process, high fabrication cost, use of toxic reagent, and poor controllability on the dispersion and durability of Cu nanoparticles, etc. Therefore, it is urgent to design and develop novel strategies for the construction of highly dispersed Cu-based catalyst with enhanced catalytic activity and stability.

As one of the most widely used catalyst supports, ZrO<sub>2</sub> has a high surface area for the dispersion of metal nanoparticles, a porous structure for the diffusion and transfer of reactants and products, and a large amount of surface Zr<sup>4+</sup>-O<sup>2-</sup> acid-base centers and oxygen vacancies for tailoring the catalytic performance [35-38]. Therefore, adjustments and optimizations of the textural properties of ZrO<sub>2</sub>, as well as the metal-support interaction between Cu and ZrO<sub>2</sub>

support, are key factors to control the dispersion, surface chemical state, and durability of Cu active components, which are essential to enhance the catalytic performance and economic feasibility of the Cu/ZrO<sub>2</sub> heterogeneous catalyst.

Based on the above consideration, we herein developed a significant strategy for the synthesis of Cu/ZrO<sub>2</sub> catalysts with highly dispersed Cu nanoparticles and large amount of Cu<sup>+</sup> catalytic centers through the reduction of evenly distributed CuO/ZrO<sub>2</sub> complex precursor, which was prepared by a novel separate nucleation and aging steps assistant reduction-oxidation route. This strategy exhibits remarkable merits: i) basic and reductive reaction conditions supplied by NaBH<sub>4</sub> and unique reduction-oxidation route can synthesize ZrO<sub>2</sub> and CuO synchronously, simplifying the preparation process; ii) explosive nucleation process in the colloid mill results in the formation of ultrafine nuclei, H<sub>2</sub> bubble generated by the hydrolysis of NaBH<sub>4</sub> in the aging step maintains the reaction system in a sustained turbulent state, and the unique reaction condition is benefit for the formation of CuO/ZrO<sub>2</sub> precursor with homogeneously distributed Cu and Zr components; iii) homogeneous dispersion of CuO, strong interaction between CuO and ZrO<sub>2</sub>, and porous structure of ZrO<sub>2</sub> support inhibit the aggregation of Cu species and lead to the formation of Cu<sup>+</sup> active centers during the reduction process. Herein, the initial NaBH<sub>4</sub> concentration plays an important role in determining the dispersion of Cu nanoparticles, surface areas of Cu<sup>0</sup>, surface Cu<sup>+</sup>/(Cu<sup>0</sup> + Cu<sup>+</sup>) molar ratio, surface acidity, and textural properties of ZrO<sub>2</sub> support. The correlation between the structure and catalytic performance of the prepared Cu/ZrO<sub>2</sub> catalyst was studied preliminarily in the transformation of GVL to corresponding alkyl valerates. It was found that the surface Cu<sup>+</sup> acted as active centers for the absorption and polarization of the carboxylic group in GVL, Cu<sup>0</sup> undertakes the dissociation of H<sub>2</sub> to produce active hydrogen for the hydrogenation step, and the cooperation of Cu<sup>+</sup> and Cu<sup>0</sup> is mainly responsible for its excellent catalytic performance. Furthermore, as formed Cu/ZrO<sub>2</sub> catalyst also showed high efficiency in the one-pot conversion of levulinic acid (LA) to pentylvalerate.

## 2. Experimental

### 2.1 Synthesis of catalyst precursors

A series of CuO/ZrO<sub>2</sub> precursors were prepared by a novel separate nucleation and aging steps assistant reduction-oxidation route. Typically, solution A: 0.5209 g Cu(NO<sub>3</sub>)<sub>2</sub>·3H<sub>2</sub>O and 4.2933 g Zr(NO<sub>3</sub>)<sub>4</sub>·5H<sub>2</sub>O were dissolved in 40 mL of deionized water to give a mixed salt solution. Solution B: NaBH<sub>4</sub> was dissolved in 40 mL of deionized water to form another solution with a designed NaBH<sub>4</sub>/(Cu + Zr) molar ratio of  $x$  ( $x = 10, 15, 20, 25$ ). Solutions A and B were simultaneously added to a colloid mill with the rotor speed set at 4000 rpm and mixed for 5 min. Then, the mixed slurry was sealed in a Teflon-lined autoclave and aged at 150 °C for 24 h, respectively. Subsequently, the resulting suspension was washed thoroughly with deionized water until pH = 7.0, and dried at 70 °C for 24 h. The obtained precursors were denoted as CuO/ZrO<sub>2</sub>- $x$ , in which  $x$  represents the molar ratio of NaBH<sub>4</sub>/(Cu + Zr).

For comparative study, CuO/ZrO<sub>2</sub>-CP and CuO/ZrO<sub>2</sub>-CH precursors were also prepared. As for CuO/ZrO<sub>2</sub>-CP, 0.5209 g Cu(NO<sub>3</sub>)<sub>2</sub>·3H<sub>2</sub>O and 4.2933 g Zr(NO<sub>3</sub>)<sub>4</sub>·5H<sub>2</sub>O were dissolved in deionized water to give a mixed salt solution, and the above salt solution was titrated with Na<sub>2</sub>CO<sub>3</sub> (0.2 M) solution under vigorous stirring at room temperature until pH = 10.0. The resulting suspension was aged at 60 °C for 10 h, and then centrifuged and washed with deionized water until pH = 7.0. The solid was dried at 70 °C for 24 h, and calcined in air at 400 °C for 4 h. CuO/ZrO<sub>2</sub>-CH was prepared by a chemisorption hydrolysis method. Typically, 1 g commercial ZrO<sub>2</sub> was ultrasonically dispersed into a 250 mL 0.007M [Cu(NH<sub>3</sub>)<sub>4</sub>]<sup>2+</sup> solution, aged at 0 °C for 6 h, and then slowly diluted with 100 mL deionized water. The obtained suspension was separated by centrifugation, washed with deionized water, dried at 70 °C for 24 h, and calcined in air at 400 °C for 4 h. In addition, CuO/SiO<sub>2</sub>-CH, CuO/MoO<sub>3</sub>-CH, and CuO/Al<sub>2</sub>O<sub>3</sub>-CH precursors were also prepared by the above chemisorption hydrolysis method using commercial acidic SiO<sub>2</sub>, MoO<sub>3</sub>, and Al<sub>2</sub>O<sub>3</sub> as support under the similar reaction conditions, respectively.

## 2.2 Synthesis of Cu-based heterogeneous catalysts

The above synthesized catalyst precursors were placed in a tube-furnace reactor, and reduced in 10 % H<sub>2</sub>/N<sub>2</sub> atmosphere at 300 °C for 2 h at a ramp rate of 2 °C min<sup>-1</sup>. The catalysts obtained from CuO/ZrO<sub>2</sub>- $x$ , CuO/ZrO<sub>2</sub>-CP, CuO/ZrO<sub>2</sub>-CH, CuO/SiO<sub>2</sub>-CH, CuO/MoO<sub>3</sub>-CH, and CuO/Al<sub>2</sub>O<sub>3</sub>-CH were denoted as Cu/ZrO<sub>2</sub>- $x$ , Cu/ZrO<sub>2</sub>-CP, Cu/ZrO<sub>2</sub>-CH, Cu/SiO<sub>2</sub>-CH,

Cu/MoO<sub>3</sub>-CH, and Cu/Al<sub>2</sub>O<sub>3</sub>-CH, respectively. All the catalysts were designed with an ideal Cu loading of 10 wt%.

### 2.3 Characterization

Powder X-ray diffraction (XRD) patterns were collected on a Bruker D8 Advance, at room temperature using Cu-K $\alpha$  radiation (40 kV, 30 mA, and K $\alpha$  = 1.5418 Å) between 20° and 80° with a scanning rate of 10° min<sup>-1</sup>.

Elemental analysis for metal ions in samples was performed using a Shimadzu ICPS-7500 inductively coupled plasma atomic emission spectroscope (ICP-AES).

Fourier transform infrared (FT-IR) spectra were recorded on a Bruker Vector 22 spectrometer using the KBr pellet technique (1mg of sample in 100 mg of KBr).

Transmission electron microscopy (TEM) and high-resolution TEM (HRTEM) were carried out on a JEOL 2100 operated at an accelerating voltage of 200 kV. High-angle annular dark-field scanning TEM-energy-dispersive X-ray spectroscopy (HAADF-STEM-EDS) images were recorded on a JEOL2010F instrument combined with an X-ray energy dispersive spectroscopy (EDS) system.

Low-temperature N<sub>2</sub> adsorption-desorption measurements were carried out at 77 K using a Micromeritics ASAP 2020 instrument. The Brunauer-Bmmett-Teller (BET) and nonlocal Density Functional Theory (NL-DFT) models were used to determine the total specific surface area and the pore size distribution of the samples, respectively.

X-ray photoelectron spectroscopy (XPS) was recorded on a Thermo VG ESCALAB250 X-ray photoelectron spectrometer using Al K $\alpha$  X-ray as the excitation source. The binding energies were calibrated based on the graphite C1s peak at 284.6 eV. X-ray induced Auger spectra (XAES) were carried out on a PHI Quantera SXM using Al K $\alpha$  X-rays as the excitation source.

Hydrogen temperature-programmed reduction (H<sub>2</sub>-TPR) and N<sub>2</sub>O titration were performed on a Mircomeritics ChemiSorb 2720, and a thermal conductivity detector (TCD) was used to determine the amount of hydrogen and N<sub>2</sub>O consumption during the test. 40 mg catalyst precursor was placed in a quartz tube and degassed in Ar atmosphere at 200 °C for 2



h. The catalyst precursor was then heated in 10 % H<sub>2</sub>-Ar at a rate of 30 mL min<sup>-1</sup> with a heating rate of 10 °C min<sup>-1</sup> from room temperature up to 800 °C. The active copper surface area was measured by the N<sub>2</sub>O oxidation method. Firstly, the catalyst precursor was reduced at 300 °C for 4 h under 10 % H<sub>2</sub>-Ar flow (30 mL min<sup>-1</sup>). After cooling to 70 °C, the gas was switched to 10 % N<sub>2</sub>O/N<sub>2</sub> with a flow rate of 40 mL min<sup>-1</sup> for 2 h. The amount of H<sub>2</sub> and N<sub>2</sub>O consumption was determined by TCD. Copper surface area was calculated by assuming a spherical shape of copper metal particles with a surface Cu density of  $1.47 \times 10^{19}$  copper atoms per m<sup>2</sup>.

NH<sub>3</sub>-TPD experiments were performed on a Micromeritics Chemi-Sorb 2720 instrument. The sample (0.1 g) was loaded into the quartz tube, degassed by heating in He at 200 °C for 1 h. The adsorption of NH<sub>3</sub> was carried out at 100 °C in an NH<sub>3</sub>-He mixture (5 vol% NH<sub>3</sub>) for 1.5 h, and then the adsorbed NH<sub>3</sub> was desorbed by raising the temperature up to 900 °C at a rate of 10 °C min<sup>-1</sup>.

#### **2.4 Catalytic tests**

Liquid phase catalytic evaluation was performed in a 100 mL high pressure reaction kettle equipped with timing heating system and a magnetic stirrer. Typically, 1 mL GVL, 0.1 g catalyst, and 20 mL alcohol solvent were charged into the reactor. Prior to the reaction, air was flushed out of the reactor, and H<sub>2</sub> was fed into the reactor at the designated pressure. Then the reactor was placed into an electric heating system which was preset to the certain reaction temperature. The reaction was initiated by starting the stirring and performed for a period of time. After reaction, the reactor was cooled with an ice-water bath for 30 min, and depressurized carefully. The products were quantified by GC (Agilent GC-7890B equipped with DB-WAX capillary column, 30.0 m × 250 μm × 0.25 μm) with a flame ionization detector by the internal standard method using dodecane. The conversion and selectivity were obtained through at least three parallel experiments. In each case, the carbon balance, calculated based on the mass difference between carbon in the introduced reactant and that in products was above 96 %. To investigate the reusability of the catalysts, the catalyst was removed from the reaction mixtures, washed with alcohol and acetone, and dried at 70 °C for 12 h. Then, fresh substrate and the recovered catalyst were employed in the repeated test.

### 3. Results and Discussion

#### 3.1 Structural characterizations

Previously, we developed a novel strategy for the synthesis of fundamentally and technologically important metal oxide ( $\text{ZrO}_2$ ,  $\text{CeO}_2$ ,  $\text{TiO}_2$ ) with high surface area, controlled pore structure, and uniform size distribution [39]. The established strategy involves rapid nucleation and the following kinetically controlled hydrothermal process, which combines the merits such as simplicity, versatility, commercial feasibility, etc. Here, we expanded the strategy to prepare homogeneously distributed  $\text{CuO/ZrO}_2$  composite, an ideal precursor for the synthesis of highly dispersed  $\text{Cu/ZrO}_2$  catalysts. Figure 1 shows the XRD patterns of  $\text{CuO/ZrO}_2$ -20 precursor (prepared with the  $\text{NaBH}_4/(\text{Cu} + \text{Zr})$  molar ratio of 20) and the resulting  $\text{Cu/ZrO}_2$ -20 catalyst after reduction. The XRD pattern of  $\text{CuO/ZrO}_2$ -20 precursor presents a series of intensive and broad (101), (110), (112), (211), and (220) diffractions of  $t$ - $\text{ZrO}_2$  crystalline phase (JCPDS No. 42-1164), and no diffractions related to  $\text{CuO}$  species were detected, indicating the homogeneous distribution nature and small particle size of  $\text{CuO}$  phase. As a contrast, new sharp  $\text{Cu}$  (111) diffraction at  $43.3^\circ$  appears in the XRD pattern of  $\text{Cu/ZrO}_2$ -20 catalyst, indicative of the presence of a face-centered cubic (fcc) metallic copper phase (JCPDS No. 04-0836). The average crystal size of metallic  $\text{Cu}$  particles estimated by the Scherrer formula according to the  $\text{Cu}$  (111) plane is about 6.2 nm. The textural property of  $\text{CuO/ZrO}_2$ -20 precursor and  $\text{Cu/ZrO}_2$ -20 catalyst was investigated by low-temperature  $\text{N}_2$  adsorption-desorption measurements (Figure S1). Both  $\text{CuO/ZrO}_2$ -20 precursor and  $\text{Cu/ZrO}_2$ -20 catalyst exhibit a combined isotherm of types I and IV with an apparent hysteresis loop in the relative pressure ( $P/P_0$ ) range of 0.4-0.8, reflecting the presence of micro/mesoporous structure. Notably, compare with  $\text{CuO/ZrO}_2$ -20 precursor, the  $\text{Cu/ZrO}_2$ -20 catalyst shows comparable surface area ( $168 \text{ m}^2 \text{ g}^{-1}$  vs.  $153 \text{ m}^2 \text{ g}^{-1}$ ) and slightly decreased total pore volume ( $0.2216 \text{ cm}^3 \text{ g}^{-1}$  vs.  $0.2178 \text{ m}^3 \text{ g}^{-1}$ ). Pore size distribution of  $\text{Cu/ZrO}_2$ -20 catalyst reveals that most of the pores lie in the diameter range of 1-10 nm, is similar to that of  $\text{CuO/ZrO}_2$ -20 precursor, reflecting high textural stability during the reduction transformation process.

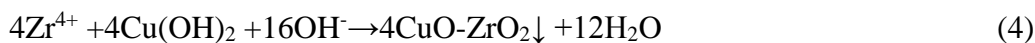
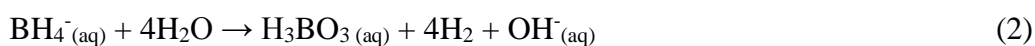
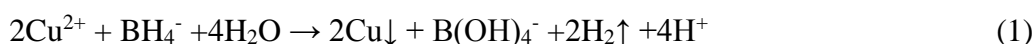
The morphology and structure of representative  $\text{Cu/ZrO}_2$ -20 catalyst was characterized by TEM and HRTEM. As shown in Figure 2a,  $\text{ZrO}_2$  support presents a porous sponge-like

framework, which is composed of interconnected spherical particle of about  $3 \pm 2$  nm in size. Due to the similar bright-dark image contrast, it causes trouble for us to distinguish the Cu particle from the  $\text{ZrO}_2$  support. A typical HRTEM image of  $\text{Cu/ZrO}_2\text{-20}$  (inset in Figure 2a) demonstrates the (111) planes of the Cu component with a  $d$ -spacing of 0.209 nm, and the (101) planes of the  $\text{ZrO}_2$  support with a  $d$ -spacing of 0.296 nm [39, 40]. Meanwhile, the blurry boundaries between metallic Cu and  $\text{ZrO}_2$  support further confirm the strong interaction between them and the homogeneously dispersed Cu particles. Further microstructural information and visual Cu dispersive nature of the synthesized  $\text{Cu/ZrO}_2\text{-20}$  catalyst were obtained from the HAADF-STEM-EDS observations. As shown in Figure 2b, semi-spherical Cu nanoparticles with an average size of 6~8 nm are distinguishable by the different contrast compared to that of  $\text{ZrO}_2$  support. The elemental mapping images of O, Cu, and Zr depict the uniform distribution of Cu and Zr in the  $\text{Cu/ZrO}_2\text{-20}$  catalyst (Figure 2c-e). Furthermore, the STEM-EDS line scan spectra of one individual particle in Figure 2g depict that Cu, O, and Zr lines show a similar Gaussian distribution along the red line in Figure 2f, indicating the homogeneous distribution and close contact in the  $\text{Cu/ZrO}_2\text{-20}$  catalyst.

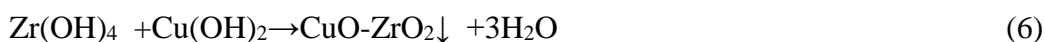
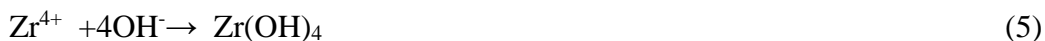
Series  $\text{Cu/ZrO}_2\text{-}x$  catalysts were also prepared with different initial  $\text{NaBH}_4/(\text{Cu} + \text{Zr})$  molar ratio. XRD patterns of  $\text{CuO/ZrO}_2\text{-}x$  precursors were shown in Figure S2. For the sample of  $\text{CuO/ZrO}_2\text{-25}$ , an additional small CuO (111) diffraction peak can be observed at around  $38.7^\circ$  with respect to that of other  $\text{CuO/ZrO}_2\text{-}x$  samples (JCPDS no. 05-0661), indicating the formation of large CuO nanoparticles in  $\text{CuO/ZrO}_2\text{-25}$  sample. Meanwhile, the XRD pattern and TEM image of the  $\text{Cu/ZrO}_2\text{-25}$  catalyst further confirm the formation of large Cu particles after reduction (Figure S3).

In our synthetic strategy,  $\text{NaBH}_4$  acts as both reductant and alkaline reagent to control the formation of  $\text{CuO/ZrO}_2$  catalyst precursor. Here, after mixing of  $\text{Zr}^{4+}$  and  $\text{Cu}^{2+}$  cations with  $\text{NaBH}_4$  reductant in a vigorously stirring colloid mill reactor, nucleation process of Cu through the reduction of  $\text{Cu}^{2+}$  cations is completed within a very short time, due to the energetic collision and strong hydraulic shear force in the highly turbulent liquid film between the stator and rotor of the colloid mill. Growth of Cu nuclei hardly takes place due to the quite short residence time in the colloid mill, and thus agglomeration of the Cu nuclei is inhibited and their sizes remain at a minimum. The XRD pattern of reduced intermediate collected from the

colloid mill only reveals the presence of amorphous phase (Figure 3a). In order to further reveal the formation mechanism, the obtained intermediate was aged for 3 h at room temperature under N<sub>2</sub> atmosphere. As shown in Figure 3b, the reduced sample exhibits broad (111), (200), and (220) diffractions of face-centered cubic (fcc) metallic copper phase, and no characteristic diffractions corresponding to metallic Zr (JCPDS No. 34-0657) or ZrO<sub>2</sub> are detected. The above results indicate a rapid nucleation of Cu in the colloid mill. In tandem with the above experimental observations, a possible formation mechanism is proposed, and the chemical reactions involved are believed to proceed as follows (eqs 1-4) [41, 42]:



In the initial step, the Cu<sup>2+</sup> cations are rapidly reduced to metallic Cu<sup>0</sup> nuclei in the colloid mill by the reductive NaBH<sub>4</sub> (eq 1). Simultaneously, OH<sup>-</sup> anions can be released into the reaction system by the hydrolysis of NaBH<sub>4</sub>, and thus raising the pH value of the aqueous reaction solution (eq 2). The newly formed Cu<sup>0</sup> nuclei are oxidized into Cu(OH)<sub>2</sub> by the trace amount of dissolved oxygen under alkaline hydrothermal conditions (eq 3). With the increase of the reaction time, the newly formed Cu(OH)<sub>2</sub> diffuses into the reaction system and reacts with Zr<sup>4+</sup> anions through a dehydration reaction under hydrothermal conditions (eq 4). Finally, through a structural transformation, CuO/ZrO<sub>2</sub> complex precursor can be obtained, in which the Cu and Zr components are evenly distributed on an atomic level without segregation of “lakes” of separate phase. However, higher NaBH<sub>4</sub> concentration may compel the reaction to proceed through a different reaction path as follows: (eq 5-6) [39]



The higher NaBH<sub>4</sub> concentration leads to the release of more sufficient OH<sup>-</sup> anions in the reaction system, Zr<sup>4+</sup> cations can also react with OH<sup>-</sup> anions to form Zr(OH)<sub>4</sub> nuclei (eq 5), and CuO/ZrO<sub>2</sub> precursor can be obtained via the dehydration of the formed Cu(OH)<sub>2</sub> and Zr(OH)<sub>4</sub> nuclei (eq 6). It should be note that eqs 4-6 may proceed concurrently. Namely, the formation path and properties of the CuO/ZrO<sub>2</sub> precursors can be simply controlled by varying

the initial NaBH<sub>4</sub> concentration.

Textural properties of series Cu/ZrO<sub>2-x</sub> catalysts were characterized by low-temperature N<sub>2</sub> adsorption-desorption measurements and listed in Table 1. Under current condition, a higher initial concentration of NaBH<sub>4</sub> leads to a higher pH value of the reaction system due to the hydrolysis of NaBH<sub>4</sub>, which is benefit for the formation and stabilization of *t*-ZrO<sub>2</sub> with higher crystallinity and larger particle size. Hence, the BET surface areas of the Cu/ZrO<sub>2-x</sub> catalyst show a decline trend with increasing the NaBH<sub>4</sub> concentration. The surface acidity of Cu/ZrO<sub>2-x</sub> catalysts was also investigated via NH<sub>3</sub>-TPD measurements. As shown in Figure S4, all the test samples exhibit a broad desorption peak at temperature range of 50-300 °C and a sharp desorption peak at temperature range of 300-450 °C, which can be assigned to the different weak acid sites and moderate strength acid sites, respectively. According to quantitative analysis on NH<sub>3</sub>-TPD results of Cu/ZrO<sub>2-x</sub> catalysts, the total acid sites decrease with increasing the initial concentration of NaBH<sub>4</sub> (Table 1), probably caused by the increased particle size and decreased surface defects of the *t*-ZrO<sub>2</sub> support. The above results indicate that the textural properties and the surface acidity of the obtained catalysts can be simply modulated by changing the NaBH<sub>4</sub> concentration during the preparation process. However, in order to get a more accurate influence mechanism of the NaBH<sub>4</sub> concentration on the prepared Cu/ZrO<sub>2-x</sub> catalyst, systemic theoretical and experimental investigations still need to be done.

H<sub>2</sub>-TPR measurements were carried out to determine the reducibility of CuO/ZrO<sub>2-x</sub> precursors. Previously studies suggested that the reduction of highly dispersed CuO to Cu<sup>0</sup> may involve a two reduction step: Cu<sup>2+</sup>→Cu<sup>+</sup>→Cu<sup>0</sup>. Due to the strong metal-support interaction, the second process of the reduction requires a higher reduction temperature than the first step [43, 44], and thus Cu<sup>+</sup> active species can be formed under mild reduction condition [45, 46]. As shown in Figure 4, there are three reduction regions for all CuO/ZrO<sub>2-x</sub> precursors in the temperature range of 150-230 °C, indicating the existence of different surface chemical state of Cu species in samples. For CuO/ZrO<sub>2-10</sub> sample, three peaks at around 175 °C, 185 °C, and 205 °C can be ascribed to the reduction of highly dispersed surface Cu species (peak I), reduction of Cu-O-Zr to Cu<sup>+</sup>-O-Zr structure (peak II), and CuO in bulk (peak III), respectively. For CuO/ZrO<sub>2-15</sub> and CuO-ZrO<sub>2-20</sub> samples, peak I and peak II shift to higher temperatures slightly, and the intensity and peak area ratio of II exhibits an increasing

trend compared to that of CuO/ZrO<sub>2</sub>-10 sample. In our synthetic strategy, the floating rate and size of the in situ generated hydrogen bubbles increase with increasing the concentration of NaBH<sub>4</sub> during the reaction process, and the violent dynamical perturbation caused by the inosculation and blast of hydrogen bubbles is benefit for the dispersion of Cu species. The highly dispersed Cu species can interact strongly with the ZrO<sub>2</sub> support, which makes Cu species much more difficult to reduce, and thus leading to slightly elevated reduction temperatures. The increased peak area ratio of II is probably caused by the formation of more Cu-O-Zr structure in the CuO/ZrO<sub>2</sub> precursor with increasing the dispersion of Cu species. Reduction peaks of bulk CuO (peak III) in CuO/ZrO<sub>2</sub>-15 and CuO-ZrO<sub>2</sub>-20 sample shift to lower temperatures, which can be ascribed to the enhancement of the dispersion of CuO in bulk, probably caused by the enhanced dynamical perturbation in the reaction system. With the further increase in the NaBH<sub>4</sub> concentration, the CuO/ZrO<sub>2</sub>-25 sample shows a reduced peak area ratio of II and increased peak area ratio of III compare to that of CuO/ZrO<sub>2</sub>-20 sample, reflecting the reduced amount of Cu-O-Zr structure and increased amount of bulk CuO in CuO/ZrO<sub>2</sub>-25 sample. In this case, though higher NaBH<sub>4</sub> concentration may result in more intensely dynamical perturbation, the increased pH value of the reaction system compels the formation of CuO/ZrO<sub>2</sub> precursor to proceed through a different reaction path, leading to the formation of large amount of bulk CuO on the ZrO<sub>2</sub> support. In addition, the formation of Cu-O-Zr structure in the prepared CuO/ZrO<sub>2</sub> precursor can be further confirmed by the appearance of additional shoulder peak at 853 cm<sup>-1</sup> with respect to that of pure ZrO<sub>2</sub> support (Figure S5). Furthermore, the appearance of an additional reduction peak in the TPR result of CuO/ZrO<sub>2</sub>-20 in the temperature range of 350-600 °C further verified the stepwise reduction of highly dispersed CuO (Figure S6). The above results demonstrate the unique reaction route and condition is benefit for the formation of Cu species with relatively high dispersion and strong metal-support interaction.

XPS and H<sub>2</sub>-N<sub>2</sub>O characterizations were carried out to confirm and quantify the surface/near-surface chemical states and Cu species in the series Cu/ZrO<sub>2</sub>-*x* catalysts. As shown in Figure 5, for all Cu/ZrO<sub>2</sub>-*x* catalysts, the appearance of a Cu 2p 3/2 signal at ca.933-935 eV and the absence of a shake-up satellite peak at 940-945 eV confirm the reduction of Cu<sup>2+</sup> species [42]. The coexistence of Cu<sup>0</sup> and Cu<sup>+</sup> species in Cu/ZrO<sub>2</sub>-*x* catalysts can be

confirmed by the appearance of a broad and asymmetric Auger kinetic energy peak in the Cu LMM XAES. The kinetic energy at ca. 916.2 eV and 918.6 eV are assigned to  $\text{Cu}^+$  species and  $\text{Cu}^0$  species, respectively. As listed in Table 1, it is interesting to note that the surface area of  $\text{Cu}^0$ ,  $\text{Cu}^+ / (\text{Cu}^0 + \text{Cu}^+)$  molar ratio, and surface Cu (including  $\text{Cu}^0$  and  $\text{Cu}^+$ ) all increase with the value of  $x$  initially and decreases afterwards, and reach their maximum when value of  $x$  is set at 20. The variation trend of the XPS results in  $\text{Cu}/\text{ZrO}_{2-x}$  catalysts is somewhat consistent with the above  $\text{H}_2$ -TPR results.

### 3.2 Catalytic performance of $\text{Cu}/\text{ZrO}_2$ catalysts

In consideration of the fact that the as-synthesized  $\text{Cu}/\text{ZrO}_2$  catalyst has a large amount of exposed active adsorption sites and reaction centers originating from high dispersion of Cu active components, as well as surface acidity and porous crystalline structure of  $\text{ZrO}_2$  support, the synthesized  $\text{Cu}/\text{ZrO}_2$  catalyst may show excellent catalytic performance in some important biomass conversion reactions. To investigate the catalytic performance of the synthesized  $\text{Cu}/\text{ZrO}_2$  catalyst, the catalytic transformation of GVL to pentyl valerate (PV) was chosen as a probe reaction.

The effects of different reaction conditions on the catalytic transformation of GVL were investigated firstly over  $\text{Cu}/\text{ZrO}_{2-20}$  catalyst using pentanol as solvent. As shown in Figure S7a, with the extension of reaction time, the conversion of GVL increases from 26.4 % to 75.7% with relatively high PV selectivity (>98.0 %) in the initial 5 h reaction period at 230 °C. The conversion reaches up to 85.4% with almost unchanged selectivity at 10 h. However, further increase the reaction time to 12 h, only results in a slightly increased GVL conversion (86.2%). If the reaction temperature is elevated from 180 °C to 230 °C, the conversion of GVL increases sharply from 15.5 % to 85.4 % because of the increased reaction rate, and the PV selectivity always maintains at a high level (98.0 %). With further increasing the reaction temperature up to 250 °C, the conversion of GVL remains constant, selectivity of PV drops to 97.2 %, 2-methyltetrahydrofuran (2-MTHF) with a selectivity of about 2.6% can be detected as the main byproduct (Figure S7b). We speculate that high reaction temperature is favor for the formation of 1, 4-pentanediol (1,4-PDO) from the hydrogenolysis of GVL and the sequential dehydration cyclization of 1,4-PDO to 2-MTHF [50,51]. Higher  $\text{H}_2$  pressure is preferable for the

conversion of GVL and the PV selectivity; nevertheless, 1,4-PDO is produced as the main byproduct when the H<sub>2</sub> pressure exceeded 2 MPa (Figure S7c). Hence, without additional remarks, 10 h of reaction time, 230 °C of reaction temperature, 1.5 MPa H<sub>2</sub> pressure are chosen as the optimized reaction conditions and performed in the following texts.

The catalytic performance of series Cu/ZrO<sub>2-x</sub> catalysts for the transformation of GVL to valerate ester was also investigated. The conversion of GVL, PV selectivity, and reaction rate  $r$  (calculated by the rate of GVL consumption per catalyst mass in the initial reaction state with GVL conversion less than 30%) were listed in Table 2. Among the series prepared Cu/ZrO<sub>2-x</sub>, Cu/ZrO<sub>2-20</sub> catalyst exhibited the best catalytic performance and the highest reaction rate, and the  $r$  value increased with the order of Cu/ZrO<sub>2-25</sub><Cu/ZrO<sub>2-10</sub><Cu/ZrO<sub>2-15</sub><Cu/ZrO<sub>2-20</sub>. In addition, the catalytic performance of Cu/ZrO<sub>2-CP</sub> and Cu/ZrO<sub>2-CH</sub> catalysts was also investigated under identical reaction conditions (Table 2 entries 5, 6), the conversion of GVL and the PV selectivity were far less than that of Cu/ZrO<sub>2-x</sub> catalysts. The low catalytic performance over the Cu/ZrO<sub>2-CP</sub> and Cu/ZrO<sub>2-CH</sub> catalysts should be assigned to the low dispersion of Cu active components (Table 1 entries 5, 6), which may be caused by the poor interaction between the CuO and ZrO<sub>2</sub> support, and the high mobility of active Cu species in the CuO/ZrO<sub>2-CP</sub> and CuO/ZrO<sub>2-CH</sub> precursors during synthesis and following reduction processes.

To clarify the origin of different catalytic performance over the synthesized Cu/ZrO<sub>2-x</sub> catalysts, systematical and comprehensive studies were carried out via correlating the physicochemical data listed in Table 1 with their catalytic performance in the catalytic transformation of GVL (Table 2). There is no much difference on the actual Cu loadings of series Cu/ZrO<sub>2-x</sub>; therefore, Cu loadings is not the origin of their different GVL transformation activities. Meanwhile, higher surface area does not correspond to superior catalytic activity, indicative of that the texture property is not the key role in determining their catalytic performance. According to literature, in most cases, surface acidity of the catalyst plays an important role in the adsorption and activation of C=O bond in GVL, and dehydration of pentyl 4-hydroxylvalerate intermediate [52]. However, in our case, there is a weak relationship between the surface acidity and the performance of the Cu/ZrO<sub>2-x</sub> catalysts, high total surface acid sites does not correlate with the high catalytic performance. It is well known that pyridine



can poison both the Brønsted acid sites and the Lewis acid sites. Hence, to further gain insight into the effect of the surface acid sites on the catalytic transformation of GVL, the poisoning test was carried out by adding pyridine in the reaction system. After the surface acid sites of the Cu/ZrO<sub>2</sub> being poisoned by pyridine, the GVL conversion dropped slightly to 73.2 % with a 95.4 % PV selectivity (Table 2, entry 7), indicating the surface acidity is benefit for the catalytic transformation of GVL but not the dominate factor under our experimental conditions. Furthermore, other acidic oxides such as SiO<sub>2</sub>, MoO<sub>3</sub>, and Al<sub>2</sub>O<sub>3</sub> were also used as support to prepare Cu-based heterogeneous catalyst for the catalytic transformation of GVL (Table 2, entries 8-10), and the GVL conversion and PV selectivity over these catalysts were inferior than that over Cu/ZrO<sub>2</sub>-CH catalyst, reflecting the positive effect of the porous ZrO<sub>2</sub> support on the catalytic transformation of GVL.

As to hydrogenation catalyzed by Cu-based catalyst, the surface Cu<sup>0</sup> plays a crucial role in the activation and dissociation of hydrogen. Figure 6 shows the variations of the reaction rate constant  $r$  in the catalytic transformation of GVL as functions of the amount of surface Cu<sup>0</sup> and surface Cu. Indeed, the highest  $r$  value of 69.6 mmol g<sub>cat</sub><sup>-1</sup> h<sup>-1</sup> is achieved over Cu/ZrO<sub>2</sub>-20 with highest amount of surface Cu<sup>0</sup>; however, the value of  $r$  does not correlate well with the surface Cu<sup>0</sup> (Figure 6a). For example,  $r$  value over Cu/ZrO<sub>2</sub>-25 is lower than that of Cu/ZrO<sub>2</sub>-10 though it has larger surface Cu<sup>0</sup>, indicating that the surface Cu<sup>0</sup> is not a sole key factor governing the performance of the catalysts. Notably, it can be found that there is a good relationship between the amount of surface Cu and the  $r$  value (Figure 6b), suggesting surface Cu<sup>+</sup> also plays an important role in the catalytic transformation of GVL to some extent. To further confirm the role of Cu<sup>+</sup> species in the catalytic transformation of GVL, Cu/ZrO<sub>2</sub>-20-600 catalyst without surface Cu<sup>+</sup> species was prepared through the reduction of CuO/ZrO<sub>2</sub>-20 precursor at 600 °C, and the sole presence of Cu<sup>0</sup> species could be confirmed by the appearance of single symmetrical peak at kinetic energy of 918.5 eV in the Cu LMM XAES of Cu/ZrO<sub>2</sub>-20-600 catalyst (Figure S8). The conversion of GVL and PV selectivity over Cu/ZrO<sub>2</sub>-20-600 catalyst drop significantly to 33.7% and 63.1%, respectively (Table 2 entry 11), even worse than that of Cu/ZrO<sub>2</sub>-25 catalyst though they have similar surface area, surface Cu<sup>0</sup>, and total acid sites (Table 1, entries 4 and 7). On the basis of the above catalytic results, we conclude that high dispersion of Cu nanoparticles, as well as cooperation of surface Cu<sup>0</sup> and Cu<sup>+</sup> are

crucial for achieving high catalytic performance in the catalytic transformation of GVL under our experimental condition.

A possible mechanism for the catalytic transformation of GVL in pentanol over the Cu/ZrO<sub>2</sub> catalysts is also proposed (Figure 7). Firstly, C=O bond in GVL can be absorbed and polarized by the surface electrophilic Cu<sup>+</sup> species, and the formed electropositive carbonyl C atom is benefit for the nucleophilic addition of electronegative hydroxyl group in pentanol, leading to the formation of pentyl 4-hydroxylvalerate intermediate. Secondly, pentyl pentenoate can be sequentially formed by the fast dehydration of pentyl 4-hydroxylvalerate [29, 53]. Finally, the highly dispersed surface Cu<sup>0</sup> active center dissociates H<sub>2</sub> to produce active hydrogen for the final hydrogenation of pentyl pentenoate to generate PV product. Cooperation between the surface Cu<sup>+</sup> and highly dispersed Cu<sup>0</sup> endows the prepared Cu/ZrO<sub>2</sub> catalyst with excellent catalytic performance in the transformation of GVL.

Heterogeneous catalysts often suffer from a decline of catalytic performance caused by the aggregation and leaching loss of active component, and the reusability of heterogeneous catalysts is a critical factor in practical catalytic application. Consequently, the reusability of the Cu/ZrO<sub>2</sub>-20 catalyst was also investigated representatively. In our case, Cu/ZrO<sub>2</sub>-20 catalyst shows a slightly reduced catalytic performance (80.0 % of GVL conversion and 97.6 % PV selectivity) after four cycles (Figure 8). Systematic characterizations of the recovered Cu/ZrO<sub>2</sub>-20-RE catalyst were carried out, and the relevant structural and component data were listed in Table 1 (Entry 8). It is revealed that the structure of the catalyst does not change after recycling four times, and no obvious agglomeration and growth of Cu particles can be observed (Figure S9 and Figure S10A). Elemental analysis by ICP-AES demonstrates that the Cu leaching loss is only about 1 wt% after recycling four times. In addition, Cu LMM XAES result shows that surface Cu<sup>+</sup>/(Cu<sup>0</sup> + Cu<sup>+</sup>) ratio decreases from 0.51 to 0.47 after four consecutive runs. (Figure S10B; Table 1, entry 8). We speculate that the slight decline of catalytic performance over the recovered Cu/ZrO<sub>2</sub>-20-RE catalyst is mainly caused by the leaching loss of Cu component and the decline of surface Cu<sup>+</sup> active sites.

To explore the range of suitable solvents for this catalytic system and the application in preparation of various alkyl valerates, series alcohols were investigated as solvents for the catalytic transformation of GVL over the Cu/ZrO<sub>2</sub>-20 catalyst. The conversion of GVL

exhibits a downward trend with the increase in the alkyl chain of the primary alcohol (Table 3, entries 1-4), and the selectivity to alkyl valerates shows a trend from decline to rise. For short-chain alcohols such as methanol and ethanol, strong polarity and weak steric hindrance are benefit for the ring-opening and addition processes, and thus leads to high GVL conversion and excellent alkyl valerates selectivity. For propanol and butanol, the subdued polarity may be responsible for the declined conversion of GVL, the increased steric hindrance may inhibit the dehydration and hydrogenation process of the formed 4-hydroxy-valerate intermediate, and propyl 4-hydroxylvalerate and butyl 4-hydroxylvalerate can be detected as main byproducts, respectively, leading to declined valerate selectivity. Though pentanol has weaker polarity and larger steric hindrance than that of butanol, the intermiscibility of GVL in pentyl is higher than that in butanol, which may be benefit for the dehydration and hydrogenation of the formed pentyl 4-hydroxylvalerate intermediate, resulting in higher pentyl valerate selectivity. In addition, the high selectivity of hexyl valerate in hexanol further confirms the above speculation to some extent (Table 3, entry 5). The conversion of GVL and selectivity to valerate ester in secondary alcohol and cyclitol is lower than that in primary alcohol (Table 3, entries 6-8). For isopropanol and isoamyl alcohol, 4-hydroxy-valerate can be detected as the main byproduct, reflecting the steric hindrance has a negative effect on the dehydration and hydrogenation of the formed 4-hydroxy-valerate intermediate [54]. For cyclohexanol, in addition to the detection of cyclohexyl 4-hydroxylvalerate, 2-MTHF can also be detected as a byproduct, which may be ascribed to the hydrogenolysis of GVL. Having established the catalytic transformation route for the production of valerate ester from GVL and alcohol, we have explored the possibility of a straight forward production of valerate ester from levulinic acid (LA), a biomass derived platform molecule. We have performed a “one-pot” process that combines the catalytic hydrogenation of LA to GVL and catalytic transformation of GVL to PV over the Cu/ZrO<sub>2</sub>-20 catalyst. The result shows that LA totally converts to GVL and the selectivity to PV reaches up to 58.7%. In future, the reaction conditions will be optimized to gain a higher yield of the target product.

#### 4. Conclusion

In summary, a cost-effective and facile strategy for the synthesis of CuO/ZrO<sub>2</sub> complex precursor has been established herein. The unique reduction-oxidation route, explosive nucleation process, and sustained perturbation at the aging step are benefit for the formation of CuO/ZrO<sub>2</sub> complex nanocrystals uniformly distributed on an atomic level, which can be used as an ideal precursor for the synthesis of Cu/ZrO<sub>2</sub> catalyst with highly dispersion of Cu and large amount of Cu<sup>+</sup> catalytic centers. It was found that the formation path and properties of CuO/ZrO<sub>2</sub> precursors, as well as the surface Cu<sup>0</sup>/(Cu<sup>0</sup> + Cu<sup>+</sup>) molar ratio of Cu/ZrO<sub>2</sub> catalyst can be simply manipulated by varying the initial NaBH<sub>4</sub> concentration. The prepared Cu/ZrO<sub>2</sub> catalysts process remarkable stability and efficiency in the catalytic transformation of GVL to pentyl valerate, which may attribute to the cooperation between Cu<sup>+</sup> and Cu<sup>0</sup> originating from enhanced metal-support interaction and highly dispersed CuO nanopartcles of the CuO/ZrO<sub>2</sub> precursors. The correlation between the catalytic performance and the surface Cu active components demonstrated that Cu<sup>+</sup> is the active site for the adsorption and polarization of GVL, while Cu<sup>0</sup> undertakes the hydrogenation of intermediates. As formed Cu/ZrO<sub>2</sub> catalyst was also efficient in straight forward production of valerate ester from biomass derived platform molecule. The present study could inspire the development of readily available, stable, highly efficient Cu-based catalyst with superior performance in the flexible conversion of bio-derived platform molecules in terms of economic and environmental sustainability.

## Acknowledgments

This work is financially supported by the National Natural Science Foundation of China and the Fundamental Research Funds for the Central Universities (buctrc 201528).

## Supplementary material

Supplementary data associated with this article can be found, in the online version, at xxxx

Low-temperature N<sub>2</sub> adsorption-desorption and pore size distribution of the CuO/ZrO<sub>2</sub>-20 precursor and Cu/ZrO<sub>2</sub>-20 catalyst; XRD patterns of series CuO/ZrO<sub>2</sub>-*x* precursors; XRD patterns of series of CuO/ZrO<sub>2</sub>-*x* precursor (a) and TEM image of Cu/ZrO<sub>2</sub>-25 catalyst (b);

NH<sub>3</sub>-TPD profiles of series Cu/ZrO<sub>2-x</sub> catalysts; FT-IR spectra of pure ZrO<sub>2</sub> (a) and CuO/ZrO<sub>2-20</sub> precursor (b); H<sub>2</sub>-TPR spectra of CuO/ZrO<sub>2-20</sub> precursor; Effect of reaction parameters on the catalytic transformation of GVL over Cu/ZrO<sub>2-20</sub> in pentanol: reaction time (a), reaction temperature (b), H<sub>2</sub> pressure (c). Reaction conditions: 1 mL GVL, 20 mL pentanol, 0.1 g catalyst; Cu 2p XPS spectra and Cu LMM XAES (inset) of Cu/ZrO<sub>2-20-600</sub> catalyst; TEM image of the recovered Cu/ZrO<sub>2-20-RE</sub>; XRD patterns (A) and Cu LMM (B) of Cu/ZrO<sub>2-20</sub> catalyst: before (a) and after (b) reaction.

## References

- [1] M. Besson, P. Gallezot, C. Pinel, *Chem. Rev.* 114 (2014) 1827-1870.
- [2] D. M. Alonso, S. G. Wettstein, J. A. Dumesic, *Chem. Soc. Rev.* 41 (2012) 8075-8098.
- [3] M. J. Climent, A. Corma, S. Iborra, *Green Chem.* 16 (2014) 516-547.
- [4] C. Perego, M. Ricci, *Catal. Sci. Technol.* 2 (2012) 1776-1786.
- [5] K. Yan, Y. Yang, J. Chai, Y. Lu, *Appl. Catal. B: Environ.* 179 (2015) 292-304.
- [6] D. Rasina, A. Lombi, S. Santoro, F. Ferlin, L. Vaccaro, *Green Chem.* 18 (2016) 6380-6386.
- [7] J. Tan, J. Cui, X. Cui, T. Deng, X. Li, Y. Zhu, Y. Li, *ACS Catal.* 5 (2015) 7379-7384.
- [8] T. M. Lima, C. G. S. Lima, A. K. Rathi, M. B. Gawande, J. Tucek, E. A. Urquieta-González, R. Zbořil, M. W. Paixão, R. S. Varma, *Green Chem.* 18 (2016) 5586-5593.
- [9] J. Ftouni, A. Muñoz-Murillo, A. Goryachev, J. P. Hofmann, E. J. M. Hensen, L. Lu, C. J. Kiely, P. C. A. Bruijninx, B. M. Weckhuysen, *ACS Catal.* 6 (2016) 5462-5472.
- [10] Y. Yang, G. Gao, X. Zhang, F. Li, *ACS Catal.* 4 (2014) 1419-1425.
- [11] O. A. Abdelrahman, A. Heyden, J. Q. Bond, *ACS Catal.* 4 (2014) 1171-1181.
- [12] Z. Yang, Y. Huang, Q. Guo, Y. Fu, *Chem. Commun.* 49 (2013) 5328-5330.
- [13] D. M. Alonso, S. G. Wettstein, J. A. Dumesic, *Green Chem.* 15 (2013) 584-595.
- [14] S. M. Sen, E. I. Gürbüz, S. G. Wettstein, D. M. Alonso, J. A. Dumesic, C. T. Maravelias, *Green Chem.* 14 (2012) 3289-3294.
- [15] J. Q. Bond, D. Wang, D. M. Alonso, J. A. Dumesic, *J. Catal.* 281 (2011) 290-299.
- [16] D. Fegyverneki, L. Orha, G. Láng, I. T. Horváth, *Tetrahedron.* 66 (2010) 1078-1081.
- [17] J. S. Luterbacher, J. M. Rand, D. M. Alonso, J. Han, J. T. Youngquist, C. T. Maravelias, B. F. Pfleger, J.

- A. Dumesic, *Science*. 343 (2014) 277-280.
- [18] L. Qi, Y. F. Mui, S. W. Lo, M. Y. Lui, G. R. Akién, I. T. Horváth, *ACS Catal.* 4 (2014) 1470-1477.
- [19] O. Casanova, S. Iborra, A. Corma, *J. Catal.* 275 (2010) 236-242.
- [20] M. Chalid, H. J. Heeres, A. A. Broekhuis, *Procedia Chemistry*. 4 (2012) 260-267.
- [21] I. T. Horváth, H. Mehdi, V. Fábos, L. Boda, L. T. Mika, *Green Chem.* 10 (2008) 238-242.
- [22] F. M. A. Geilen, B. Engendahl, A. Harwardt, W. Marquardt, J. Klankermayer, W. Leitner, *Angew. Chem. Int. Ed.* 49 (2010) 5510-5514.
- [23] M. G. Al-Shaal, A. Dzierbinski, R. Palkovits, *Green Chem.* 16 (2014) 1358-1364.
- [24] M. Pagliaro, R. Ciriminna, H. Kimura, M. Rossi, C. D. Pina, *Angew. Chem. Int. Ed.* 46 (2007) 4434-4440.
- [25] K. Kon, W. Onodera, K. Shimizu, *Catal. Sci. Technol.* 4 (2014) 3227-3234.
- [26] J. P. Lange, R. Price, P. M. Ayoub, J. Louis, L. Petrus, L. Clarke, H. Gosselink, *Angew. Chem. Int. Ed.* 49 (2010) 4479-4483.
- [27] P. Sun, G. Gao, Z. Zhao, C. Xia, F. Li, *ACS Catal.* 4 (2014) 4136-4142.
- [28] N. Scotti, M. Dangate, A. Gervasini, C. Evangelisti, N. Ravasio, F. Zaccheria, *ACS Catal.* 4 (2014) 2818-2826.
- [29] C. E. Chan-Thaw, M. Marelli, R. Psaro, N. Ravasio, F. Zaccheria, *RSC Adv.* 3 (2013) 1302-1306.
- [30] L. Wang, Q. Liu, M. Chen, Y. Liu, Y. Cao, H. He, K. Fan, *J. Phys. Chem. C.* 111 (2007) 16549-16557.
- [31] S. Proding, M. A. Derewinski, Y. Wang, N. M. Washton, E. D. Walter, J. Szanyi, F. Gao, Y. Wang, C. H. F. Peden, *Appl. Catal. B: Environ.* 201 (2017) 461-469.
- [32] X. Dong, F. Lia, N. Zhao, F. Xiao, J. Wang, Y. Tan, *Appl. Catal. B: Environ.* 191 (2016) 8-17.
- [33] P. Mierczynski, K. Vasilev, A. Mierczynska, W. Maniukiewicz, M. I. Szyrkowska, T. P. Maniecki, *Appl. Catal. B: Environ.* 185 (2016) 281-294.
- [34] M. Meng, Y. Liu, Z. Sun, L. Zhang, X. Wang, *Int. J. Hydrogen Energy.* 37 (2012) 14133-14142.
- [35] Y. Bie, J. Lehtonen, J. Kanervo, *Appl. Catal. A: Gen.* 526 (2016) 183-190.
- [36] H. Chen, Y. Wu, S. Qi, Y. Chen, M. Yang, *Appl. Catal. A: Gen.* 529 (2017) 79-90.
- [37] J. Luo, H. Xu, Y. Liu, W. Chu, C. Jiang, X. Zhao, *Appl. Catal. A: Gen.* 423-424 (2012) 121-129.
- [38] S. Esposito, M. Turco, G. Bagnasco, C. Cammarano, P. Pernice, A. Aronne, *Appl. Catal. A: Gen.* 372 (2010) 48-57.
- [39] W. Cao, J. Kang, G. Fan, L. Yang, F. Li, *Ind. Eng. Chem. Res.* 54 (2015) 12795-12804.

- [40] Q. Hu, G. Fan, L. Yang, F. Li, *ChemCatChem*. 6 (2014) 3501-3510.
- [41] G. Fan, F. Li, *Chem. Eng. J.* 167 (2011) 388-396.
- [42] Z. Gu, X. Xiang, G. Fan, F. Li, *J. Phys. Chem. C*. 112 (2008) 18459-18466.
- [43] Q. Hu, L. Yang, G. Fan, F. Li, *J. Catal.* 340 (2016) 184-195.
- [44] X. Ma, H. Chi, H. Yue, Y. Zhao, Y. Xu, J. Lv, S. Wang, J. Gong, *AIChE J.* 59 (2013) 2530-2539.
- [45] L. Chen, P. Guo, M. Qiao, S. Yan, H. Li, W. Shen, H. Xu, K. Fan, *J. Catal.* 257 (2008) 172-180.
- [46] Z. He, H. Lin, P. He, Y. Yuan, *J. Catal.* 277 (2011) 54-63.
- [47] A. J. Marchi, J. L. G. Fierro, J. Santamaría, A. Monzón, *Appl. Catal. A: General*. 142 (1996) 375-386.
- [48] J. Gong, H. Yue, Y. Zhao, S. Zhao, L. Zhao, J. Lv, S. Wang, X. Ma, *J. Am. Chem. Soc.* 134 (2012) 13922-13925.
- [49] S. Zhang, G. Fan, F. Li, *Green Chem.* 15 (2013) 2389-2393.
- [50] X. Du, Q. Bi, Y. Liu, Y. Cao, H. He, K. Fan, *Green Chem.* 14 (2012) 935-939.
- [51] D. Ren, X. Wan, F. Jin, Z. Song, Y. Liu, Z. Huo, *Green Chem.* 18 (2016) 5999-6003.
- [52] W. Li, Y. Li, G. Fan, L. Yang, F. Li, *ACS Sustainable Chem. Eng.* 5 (2017) 2282-2291.
- [53] K. Yan, T. Lafleur, X. Wu, J. Chai, G. Wu, X. Xie, *Chem. Commun.* 51 (2015) 6984-6987.
- [54] T. Pan, J. Deng, Q. Xu, Y. Xu, Q. Guo, Y. Fu, *Green Chem.* 15 (2013) 2967-2974.

## Table

**Table 1.** The structural and component data of different catalysts.

Entry	Samples	Cu (wt %) <sup>a</sup>	S <sub>BET</sub> (m <sup>2</sup> g <sup>-1</sup> ) <sup>b</sup>	Total acid sites (mmol g <sup>-1</sup> ) <sup>c</sup>	D <sub>111</sub> <sup>d</sup> (nm)	S <sub>Cu</sub> (m <sup>2</sup> g <sup>-1</sup> ) <sup>e</sup>	Cu <sup>+</sup> / (Cu <sup>0</sup> + Cu <sup>+</sup> ) <sup>f</sup>	Surface Cu <sup>0</sup> (μmol g <sup>-1</sup> ) <sup>e</sup>	Surface Cu (μmol g <sup>-1</sup> ) <sup>g</sup>
1	Cu/ZrO <sub>2</sub> -10	9.6	192	0.88	7.8	6.0	0.44	145	258
2	Cu/ZrO <sub>2</sub> -15	9.5	158	0.79	7.4	6.8	0.45	164	298
3	Cu/ZrO <sub>2</sub> -20	9.7	153	0.61	6.2	7.4	0.51	179	363
4	Cu/ZrO <sub>2</sub> -25	9.9	168	0.52	8.7	6.2	0.39	151	248
5	Cu/ZrO <sub>2</sub> -CP <sup>h</sup>	9.9	104	0.54	8.5	3.6	0.34	89	134
6	Cu/ZrO <sub>2</sub> -CH <sup>i</sup>	9.6	53	0.37	10.3	2.1	0.26	52	70
7	Cu/ZrO <sub>2</sub> -20-600 <sup>j</sup>	9.7	152	0.43	9.0	6.8	0.05	166	174
8	Cu/ZrO <sub>2</sub> -20-RE <sup>k</sup>	9.6	157	0.64	6.6	8.0	0.47	190	358

<sup>a</sup> Determined by ICP-AES.

<sup>b</sup> Specific surface area calculated by the BET method.

<sup>c</sup> Determined by NH<sub>3</sub>-TPD analysis.

<sup>d</sup> Crystallite size based on XRD line broadening of the (111) plane for Cu metal.

<sup>e</sup> Metallic copper surface area determined by H<sub>2</sub>-N<sub>2</sub>O titration.

<sup>f</sup> Determined by Cu XAES analysis.

<sup>g</sup> Deduced from metallic copper surface area and Cu XAES results.



- <sup>h</sup> Cu/ZrO<sub>2</sub>-CP catalyst prepared by co-precipitation method
- <sup>i</sup> Cu/ZrO<sub>2</sub>-CH catalyst prepared by chemisorption hydrolysis method.
- <sup>j</sup> Cu/ZrO<sub>2</sub>-20-600 catalyst reduced in H<sub>2</sub> at 600 °C for 4 h.
- <sup>k</sup> Cu/ZrO<sub>2</sub>-20 catalyst recycled for 4 times.

**Table 2.** Transformation of GVL to pentyl valerate over various catalysts. <sup>a</sup>

Entry	Catalysts	Conversion (%)	Selectivity (%)			$r$ (mmol g <sub>cat</sub> <sup>-1</sup> h <sup>-1</sup> ) <sup>b</sup>
			PV	2-MTHF	Others	
1	Cu/ZrO <sub>2</sub> -10	39.5	98.1	0.9	1.0	44.4
2	Cu/ZrO <sub>2</sub> -15	60.9	97.7	1.2	1.1	52.1
3	Cu/ZrO <sub>2</sub> -20	85.4	98.1	1.0	0.9	69.6
4	Cu/ZrO <sub>2</sub> -25	66.2	97.8	1.2	1.0	36.2
5	Cu/ZrO <sub>2</sub> -CP	37.5	62.1	28.4	9.5	24.9
6	Cu/ZrO <sub>2</sub> -CH	25.4	56.7	29.7	13.6	18.3
7	Cu/ZrO <sub>2</sub> -20-py <sup>c</sup>	73.2	95.4	2.2	2.4	59.6
8	Cu/SiO <sub>2</sub> -CH	9.3	7.1	91.8	1.0	5.0
9	Cu/MoO <sub>3</sub> -CH	24.2	16.3	83.0	0.7	17.1
10	Cu/Al <sub>2</sub> O <sub>3</sub> -CH	14.5	10.4	88.5	1.1	9.9
11	Cu/ZrO <sub>2</sub> -20-600	33.7	63.1	25.3	11.6	23.6
12	Cu/ZrO <sub>2</sub> -20-RE <sup>d</sup>	83.00	97.6	1.6	0.8	65.5

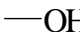
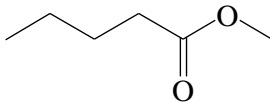
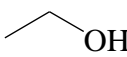
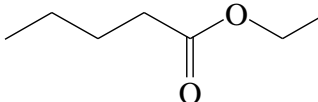
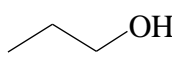
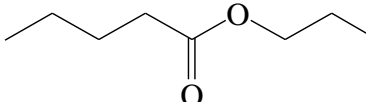
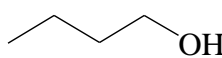
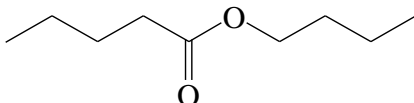
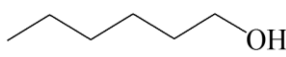
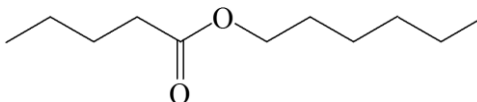
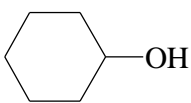
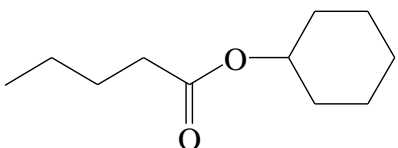
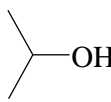
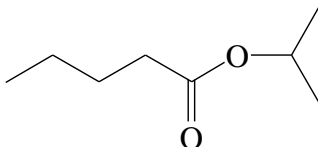
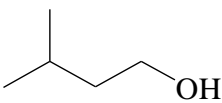
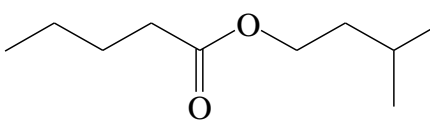
<sup>a</sup> Reaction conditions: 1 mL GVL, 20 mL pentanol, 0.1 g catalyst, reaction temperature 230 °C, reaction time 10 h, and 1.5 MPa H<sub>2</sub> pressure.

<sup>b</sup> Calculated by the rate of GVL consumption per catalyst mass in the initial reaction state with GVL conversion less than 30%.

<sup>c</sup> Cu/ZrO<sub>2</sub>-20 catalyst poisoned by pyridine.

<sup>d</sup> Cu/ZrO<sub>2</sub>-20 catalyst reused for 4 times.

**Table 3.** Catalytic performance of Cu/ZrO<sub>2</sub>-20 catalyst for the transformation of GVL in different alcohol solvents. <sup>a</sup>

Entry	Solvent & reactant	Products	Conversion	Selectivity
1			95.6%	92.4%
2			92.4%	90.0%
3			90.0%	74.9%
4			87.6%	75.2%
5			72.5%	94.8 %
6			69.3%	41.9%
7			82.5%	52.7%
8			79.0%	45.5%

<sup>a</sup> Reaction condition: 1 mL GVL, 20 mL solvent, 0.1 g catalyst, reaction temperature 230 °C, reaction time 10 h, and H<sub>2</sub> pressure 1.5 MPa.

## Figures and captions

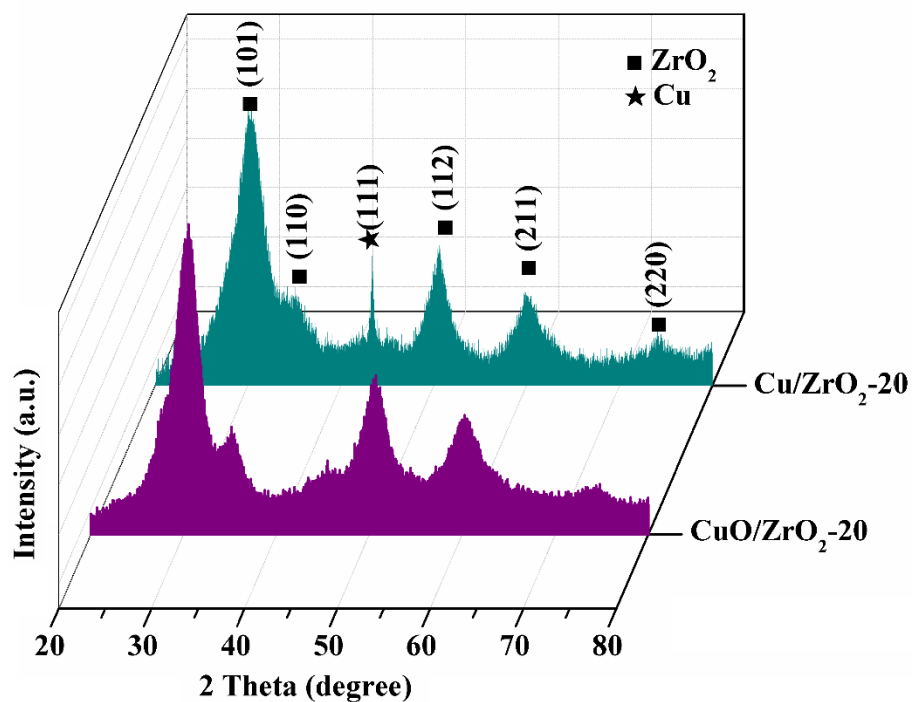


**Figure 1** XRD patterns of CuO/ZrO<sub>2</sub>-20 precursor and corresponding Cu/ZrO<sub>2</sub>-20 catalyst after reduction.

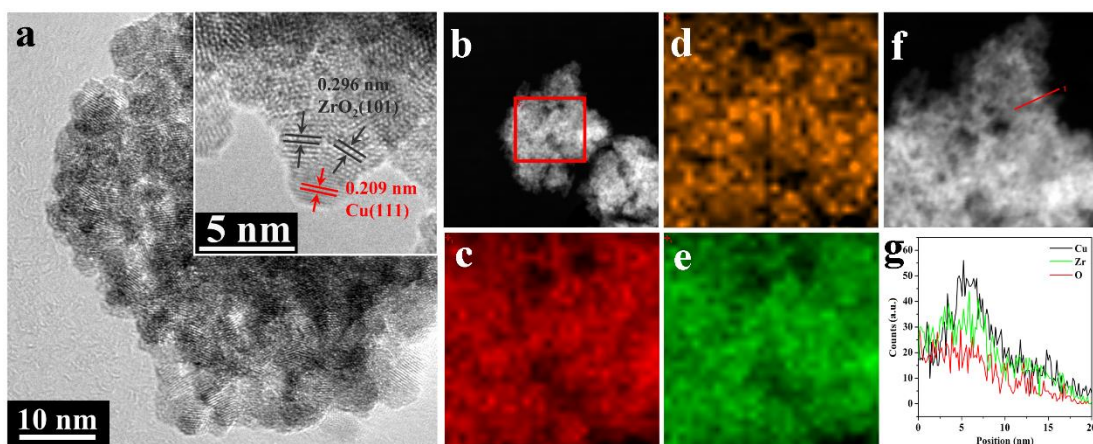


**Figure 2** HRTEM images (a) of Cu/ZrO<sub>2</sub>-20 catalyst; HAADF-STEM image (b) of Cu/ZrO<sub>2</sub>-20 with EDX mappings of O (c), Cu (d) and Zr (e); High-magnification STEM image (f); EDX line spectra of CuK, ZrK, and OK along the red line in f (g).

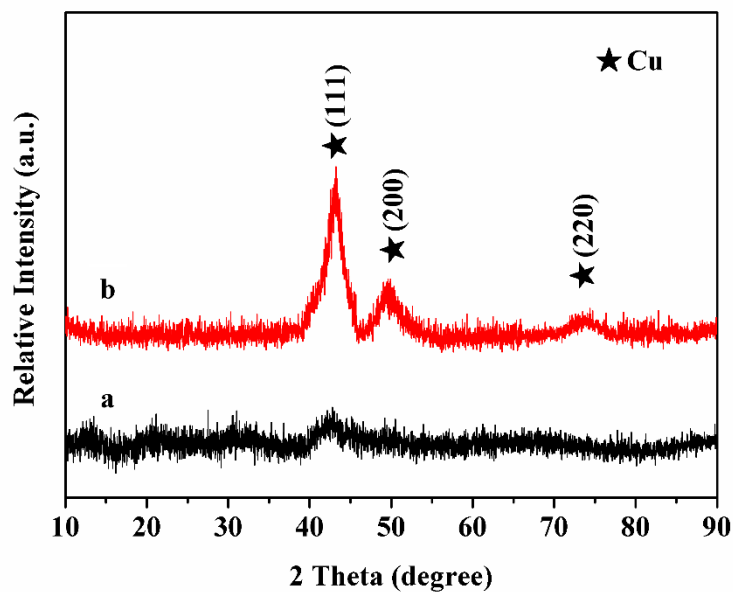


**Figure 3** XRD patterns for reduced immediate products in the colloid mill (a) without aging and (b) aging for 3 h at room temperature under  $N_2$  atmosphere.

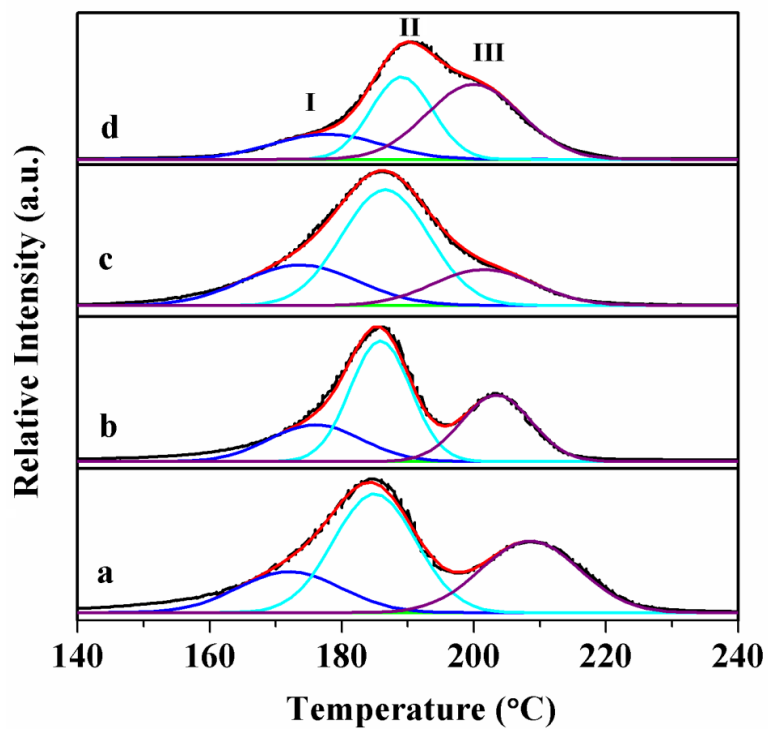


**Figure 4**  $H_2$ -TPR spectra of  $CuO/ZrO_{2-x}$  precursors prepared with different initial  $NaBH_4/(Cu+Zr)$  molar of  $x$ : a=10, b=15, c=20, d=25.

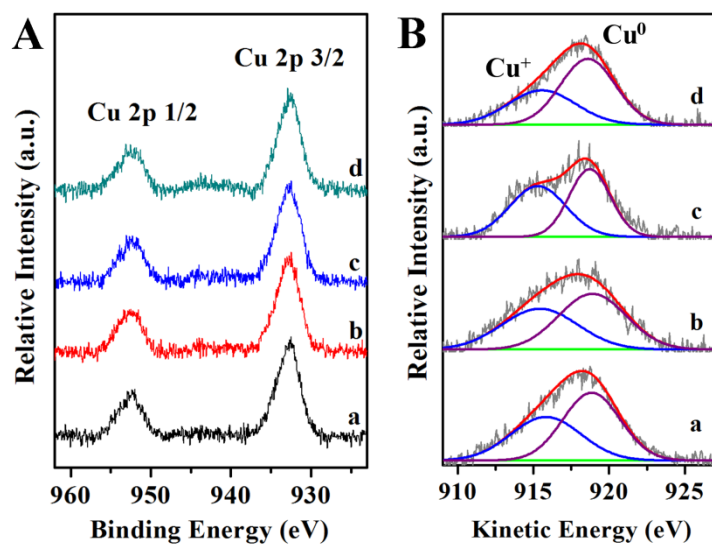


**Figure 5** Cu 2p XPS spectra (A) and Cu LMM XAES (B) of Cu/ZrO<sub>2-x</sub> with different initial NaBH<sub>4</sub>/(Cu+Zr) molar of  $x$ : a=10, b=15, c=20, d=25.

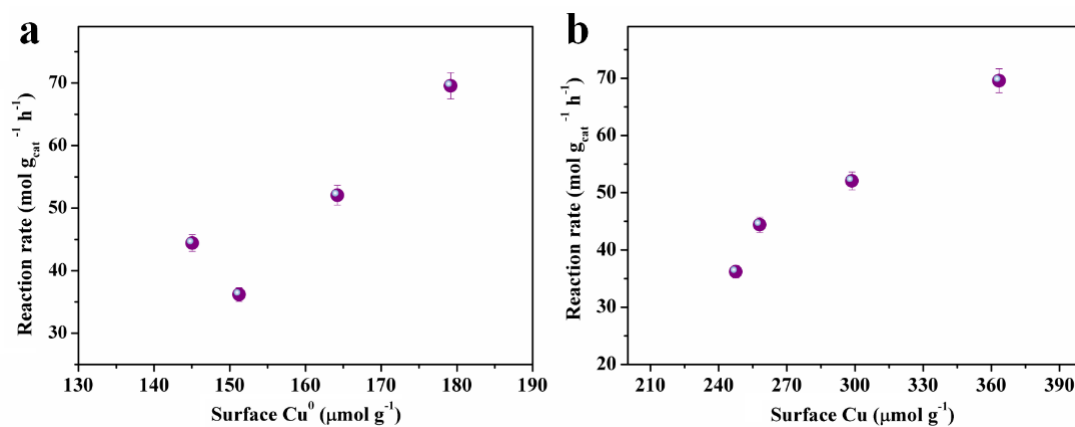


**Figure 6** The  $r$  value as a function of surface Cu<sup>0</sup> (a) and surface Cu (b) for catalytic transformation of GVL over series Cu/ZrO<sub>2-x</sub> catalyst.

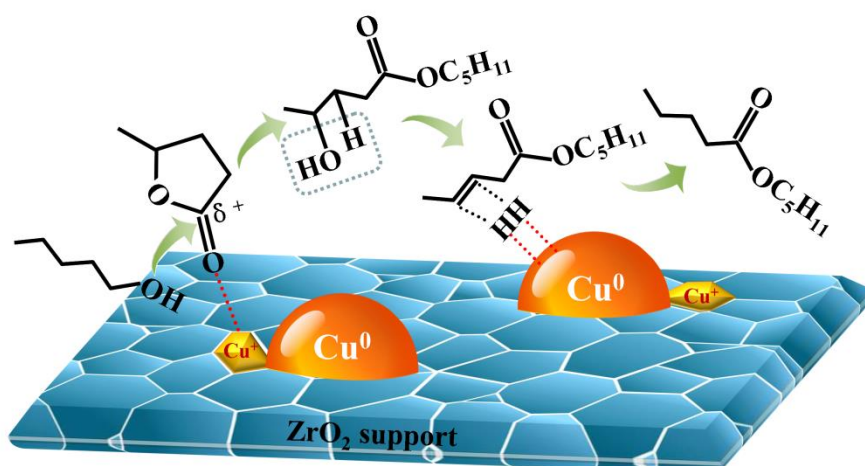


**Figure 7** Proposed simplified catalytic transformation of GVL on Cu/ZrO<sub>2</sub> catalysts.

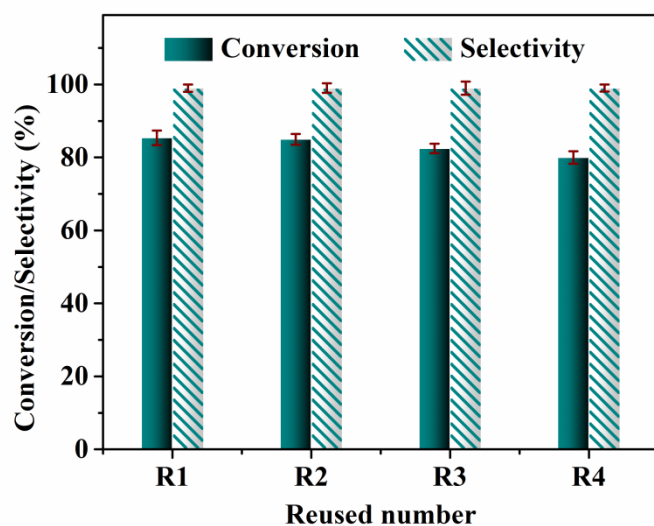


**Figure 8** Recyclability of Cu/ZrO<sub>2</sub>-20 in the catalytic transformation of GVL. Reaction conditions: 1 mL GVL, 20 mL pentanol, 0.1 g catalyst, reaction temperature 230 °C, reaction time 10 h, and 1.5 MPa H<sub>2</sub> pressure.